# Hexagonal wavelet processing of digital mammography

Andrew Laine and Sergio Schuler

University of Florida
Computer and Information Sciences Department
Computer Sciences and Engineering Building, Room 301
Gainesville, Fl 32611

Walter Huda, Janice Honeyman
and Barbara Steinbach

University of Florida
Department of Radiology
Gainesville, Fl 32610

## ABSTRACT

This paper introduces a novel approach for accomplishing mammographic feature analysis through overcomplete multiresolution representations. We show that efficient representations may be identified from digital mammograms and used to enhance features of importance to mammography within a continuum of scale-space. We present a method of contrast enhancement based on an overcomplete, non-separable multiscale representation: The hexagonal wavelet transform.

Mammograms are reconstructed from transform coefficients modified at one or more levels by local and global non-linear operators. Multiscale edges identified within distinct levels of transform space provide local support for enhancement. In addition, we show that transform coefficients, modified (globally within each level) by an adaptive non-linear operator (histogram specification), can make more obvious unseen or barely seen features of mammography without requiring additional radiation. In each case, multiscale edges and gain parameters are identified adaptively by the measure of energy within each level of scale-space.

We demonstrate that features extracted from multiresolution representations can provide an adaptive mechanism for accomplishing local contrast enhancement. We suggest that multiscale detection and local enhancement of singularities may be effectively employed for the visualization of breast pathology without excessive noise amplification. By improving the visualization of breast pathology we can improve chances of early detection (improve quality) while requiring less time to evaluate mammograms for most patients (lower costs).

## 1. INTRODUCTION

Many cancers escape detection due to the density of surrounding breast tissue. For example, differences in attenuation of the various soft tissue structures in the female breast are small, and it is necessary to use low levels of X-ray energy to obtain high contrast in mammographic film. Since contrast between the soft tissues of the breast is inherently low and because relatively minor changes in mammary structure can signify the presence of a malignant breast tumor, the detection is more difficult in mammography than in most other forms of radiography. The radiologist must search for malignancy in mammographic features such as microcalcifications, dominate and stellate masses, as well as textures of fibrous tissues (fibroglandular patterns).

A primary breast carcinoma can metastasize when it consists of a relatively small number of cells, far below our present threshold of detection. The importance of diagnosis of breast cancer at an early stage is critical to patient survival. Despite advances and improvements in mammography and mammographic screening programs, the detection of minimal breast cancer (those cancers 1.0 cm or less in diameter) remains difficult. At present, mammography is capable of detecting some cases through indirect signs, particularly through the presence of characteristic microcalcifications. It has been suggested that as normally viewed, mammograms display only about 3% of the information they detect! [1]. The inability to detect these small tumors motivates the multiscale imaging techniques presented in this paper.

0-8194-1131-0/93/$6.00



Downloaded from SPIE Digital Library on 30 Aug 2010 to 128.59.161.30. Terms of Use: http://spiedl.org/terms

Digital image processing techniques have been applied previously to mammography. The focus of past investigations has been to enhance mammographic features while reducing the enhancement of noise. Gordon and Rangayyan [9] used adaptive neighborhood image processing to enhance the contrast of features relevant to mammography. This method enhanced the contrast of mammographic features as well as noise and digitization effects. Dhawan [6, 7, 8] has made significant contributions towards solving problems encountered in mammographic image enhancement. He developed an adaptive neighborhood-based image processing technique that utilized low-level analysis and knowledge about a desired feature in the design of a contrast enhancement function to improve the contrast of specific features. Recently, Tahoces [26] developed a method for the enhancement of chest and breast radiographs by automatic spatial filtering. In their method, they used a linear combination of an original image and two smoothed images obtained from the original image by applying different spatial masks. The process was completed by nonlinear contrast stretching. This spatial filtering enhanced edges while minimally amplifying noise.

Methods of feature enhancement have been key to the success of classification algorithms. Lai [10] compared several image enhancement methods for detecting circumscribed masses in mammograms. They compared an edge-preserving smoothing function [22], a half-neighborhood method [23], k-nearest neighborhood, directional smoothing [5] and median filtering [2], and in addition proposed a method of selective median filtering.

In the fields of image processing and computer vision, transforms such as windowed Fourier transforms that can decompose a signal into a set of frequency intervals of constant size have been applied to many applications, including image compression and texture analysis. Because the spatial and frequency resolutions of these transforms remain fixed, the information provided by such transforms is not local within each interval. A wavelet transform [3, 4, 16, 17, 18, 19] is a decomposition of a signal onto a family of functions called a wavelet family. It decomposes an image onto a set of frequency channels having a constant bandwidth in logarithmic scale. The wavelet transform provides a precise understanding of the concept of multiresolution. In wavelet analysis, the variation of resolution enables transform coefficients to focus on the irregularities of a signal and characterize them locally.

In this paper we introduce a novel method for accomplishing adaptive contrast enhancement [11, 12, 13]. We describe a method of image enhancement that uses non-separable analyzing functions to compute a multiscale representations. Mammograms are then reconstructed from transform coefficients modified at each level by local and global non-linear operators. We show preliminary results that suggest such methods can emphasize significant features in digital mammography and improve the visualization of breast pathology.

## 2. OVERCOMPLETE REPRESENTATIONS FOR MULTISCALE ANALYSIS

The novelty of our approach includes the application of wavelet transforms to accomplish multiscale feature analysis and detection. Using wavelets as a set of basis functions, we may decompose an image into a multiresolution hierarchy of localized information at different spatial frequencies. Wavelet bases are more attractive than traditional hierarchical bases because they are orthonormal (traditionally), linear, continuous, and continuously invertible. The multiscale representation of wavelet transforms suggest a mathematically coherent basis not only for existing multi-grid techniques, but also for embedding non-linear methods. We suggest that these representations may increase the capacity and reliability of autonomous systems to accomplish classification of known abnormalities.

In contrast to ad-hoc approaches, the methods presented in this paper suggest the development of a practical diagnostic tool embedded in a unified mathematical theory. By this virtue, wavelet methods can exceed the performance of previous multiresolution techniques that have relied mostly on traditional methods of time-frequency analysis such as the Wigner distribution (1932) and Gabor's sliding-window (1946) transforms.

The multiresolution wavelet representation provides a natural hierarchy in which to embed an interactive paradigm for accomplishing scale-space feature analysis. Similar to traditional coarse to fine matching strategies, the radiologist may first choose to look for coarse features (e.g. dominant masses) within low frequency levels of the wavelet transform and later examine finer features (e.g. microcalcifications) at



Downloaded from SPIE Digital Library on 30 Aug 2010 to 128.59.161.30. Terms of Use: http://spiedl.org/terms

higher frequency levels. Choosing wavelets (or analyzing functions) that are simultaneously localized in both space and frequency, results in a powerful methodology for image analysis. The inner-product of a signal $f$ with a wavelet $\psi$ $\left(\langle f, \psi \rangle = (2\pi)^{-1} \left\langle \hat{f}, \hat{\psi} \right\rangle\right)$ reflects the character of $f$ within the time-frequency region where $\psi$ is localized ($\hat{\psi}$ and $\hat{f}$ are the Fourier transforms of the analyzing function and the signal, respectively). If $\psi$ is spatially localized, then two-dimensional features such as shape and orientation are preserved in the transform space and may characterize a feature through scale-space. We may "extract" such features by applying geometric constraints within each level of the transform. We reduce the complexity of the reconstructed mammogram by selecting a subset of features that satisfy certain geometric constraints. For example, we may choose to focus on only those features oriented in the horizontal direction. Subsequent image reconstructions may use the context provided by previously enhanced features to examine (diagnose) additional features emergent at other scales and orientations. Thus, fine vertical features may be selected and analyzed in the context of previously classified large horizontal features. Our strategy provides a global context upon which subtle features within finer scales may be classified incrementally through a precomputed hierarchy of scale-space.

Our approach to feature analysis and classification is motivated in part by recently discovered biological mechanisms of the human visual system [28]. Both multiorientation and multiresolution are known features of the human visual system. There exist cortical neurons which respond specifically to stimuli within certain orientations and frequencies. In practice we exploit the mathematical properties of wavelet transforms including linearity, continuity, and continuous invertibility to make features more obvious. In the next section we show these properties can accomplish adaptive contrast enhancement of digital mammography.

## 3. HEXAGONAL SAMPLING SYSTEMS

Let $x_a(\mathbf{t}) = x_a(t_1, t_2)$ be a 2-D analog waveform, then a sampling operation in 2-D can be represented by a lattice formed by taking all integer linear combinations of a set of two linearly independent vectors $\mathbf{v}_1 = [v_{11}\ v_{21}]^{\mathrm{T}}$ and $\mathbf{v}_2 = [v_{12}\ v_{22}]^{\mathrm{T}}$. Using vector notation we can represent the lattice as the set of all vectors $\mathbf{t} = [t_1\ t_2]^{\mathrm{T}}$ generated by

$$\mathbf{t} = \mathbf{V}\mathbf{n}, \tag{1}$$

where $\mathbf{n} = [n_1\ n_2]^{\mathrm{T}}$ is an integer-valued vector and $\mathbf{V} = [\mathbf{v}_1\ \mathbf{v}_2]$ is a $2 \times 2$ matrix, known as the *sampling matrix*. Because $\mathbf{v}_1$ and $\mathbf{v}_2$ are chosen to be linearly independent, the determinant of $\mathbf{V}$ is nonzero. Note that $\mathbf{V}$ is not unique for a given sampling pattern and that the two matrices representing the same sampling process are related by a linear transformation represented by a unimodular matrix [15].

Sampling an analog signal $x_a(\mathbf{t})$ on the lattice defined by (1) produces the discrete signal $x(\mathbf{n}) = x_a(\mathbf{V}\mathbf{n})$. Figure 1(a) shows a hexagonal sampling lattice defined by the pair of sampling vectors

$$\mathbf{v}_1 = \begin{bmatrix} 2T_1 \\ 0 \end{bmatrix} \text{ and } \mathbf{v}_2 = \begin{bmatrix} -T_1 \\ T_2 \end{bmatrix}, \tag{2}$$

where $T_1 = \frac{1}{2}$ and $T_2 = \frac{\sqrt{3}}{2}$. The lattice is hexagonal since each sample location has exactly six nearest neighbors when $T_2 = T_1\sqrt{3}$.

Let the Fourier transform of $x_a(\mathbf{t})$ be defined by

$$X_a(\mathbf{\Omega}) = \int_{-\infty}^{+\infty} x_a(\mathbf{t}) \exp(-j\mathbf{\Omega}^{\mathrm{T}}\mathbf{t}) d\mathbf{t},$$

where $\mathbf{\Omega} = [\Omega_1\ \Omega_2]^{\mathrm{T}}$. Similarly, let the Fourier transform of the sequence $x(\mathbf{n})$ be defined as

$$X(\omega) = \sum_{\mathbf{n}} x(\mathbf{n}) \exp(-j\omega^{\mathrm{T}}\mathbf{n}), \tag{3}$$



Downloaded from SPIE Digital Library on 30 Aug 2010 to 128.59.161.30. Terms of Use: http://spiedl.org/terms

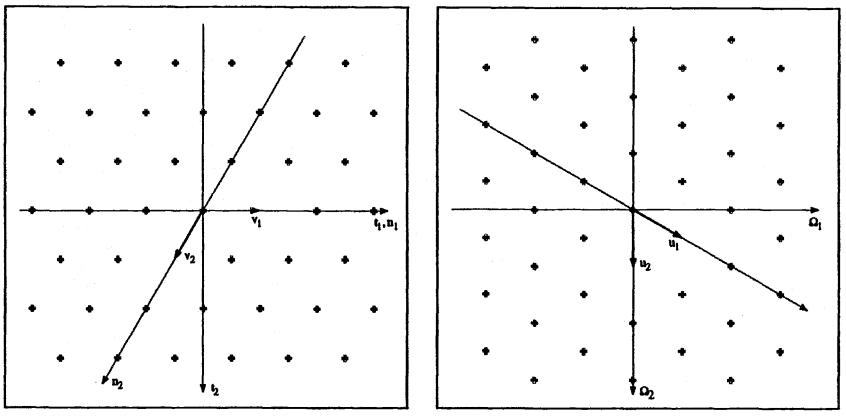

(a) (b)

Figure 1: (a) A hexagonal sampling lattice in the spatial domain. (b) Hexagonal sampling lattice in the frequency domain.

where $\boldsymbol{\omega} = [\omega_1 \ \omega_2]^{\mathrm{T}}$. In [20], Mersereau showed that the spectrum of the sequence $x(\mathbf{n})$ and the spectrum of the signal $x_a(\mathbf{t})$ are related by

$$X(\boldsymbol{\omega}) = \frac{1}{|\det \mathbf{V}|} \sum_{\mathbf{k}} X_a(\mathbf{V}^{-\mathrm{T}}(\boldsymbol{\omega} - 2\pi\mathbf{k})), \tag{4}$$

where $\mathbf{k}$ is an integer-valued vector and $\mathbf{V}^{-\mathrm{T}}$ denotes $(\mathbf{V}^{-1})^{\mathrm{T}}$. Alternatively, we can define the Fourier transform of the sequence $x(\mathbf{n})$ as

$$X_{\mathrm{V}}(\boldsymbol{\Omega}) \ = \ X(\mathbf{V}^{\mathrm{T}}\boldsymbol{\Omega}), \tag{5}$$

then equation (4) may be written as

$$X_{\mathrm{V}}(\boldsymbol{\Omega}) = \frac{1}{|\det \mathbf{V}|} \sum_{\mathbf{k}} X_a(\boldsymbol{\Omega} - \mathbf{U}\mathbf{k}), \tag{6}$$

where

$$\mathbf{U} = 2\pi\mathbf{V}^{-\mathrm{T}}. \tag{7}$$

Thus, equation (6) can be interpreted as a periodic extension of $X_a(\boldsymbol{\Omega})$ with periodicity vectors $\mathbf{u}_1 = [u_{11} \ u_{21}]^{\mathrm{T}}$ and $\mathbf{u}_2 = [u_{12} \ u_{22}]^{\mathrm{T}}$, where $\mathbf{U} = [\mathbf{u}_1 \ \mathbf{u}_2]$. The set of all vectors $\boldsymbol{\Omega}$ generated by $\boldsymbol{\Omega} = \mathbf{U}\mathbf{n}$ defines a lattice in the frequency domain known as the modulation or reciprocal lattice. Thus, the spectrum of a sequence $x(\mathbf{n})$ can be viewed as the convolution of the spectrum of $x_a(\mathbf{t})$ with a modulation lattice defined by $\mathbf{U}$. Figure 1(b) shows the reciprocal lattice corresponding to the sampling vectors defined in equation (2), that is the lattice defined by the pair of modulation vectors

$$\mathbf{u}_1 \ = \ \begin{bmatrix} \frac{\pi}{T_1} \\ \frac{\pi}{T_2} \end{bmatrix} \text{ and } \mathbf{u}_2 \ = \ \begin{bmatrix} 0 \\ \frac{2\pi}{T_2} \end{bmatrix}.$$

Two important operations in analysis/synthesis filter banks are upsampling and downsampling. Next, we consider these operations in the context of hexagonal sampling systems.



Downloaded from SPIE Digital Library on 30 Aug 2010 to 128.59.161.30. Terms of Use: http://spiedl.org/terms

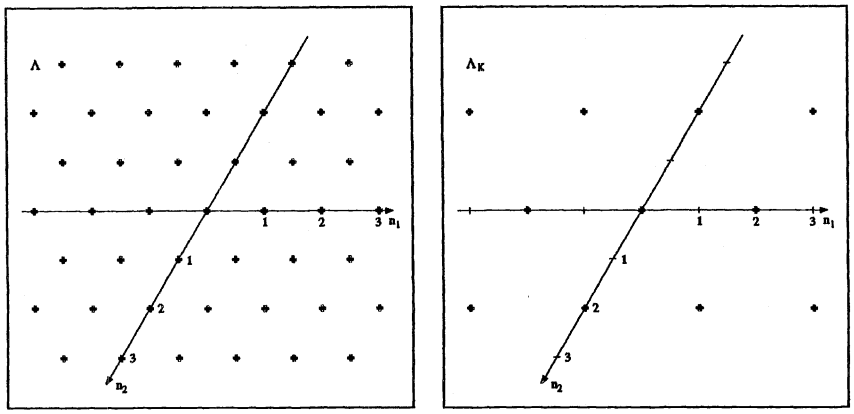


(a) (b)

Figure 2: (a) Integer sampling lattice. (b) Sampling sublattice.

## 4. UPSAMPLING AND DOWNSAMPLING IN HEXAGONAL SYSTEMS

Let $\Lambda$ denote the integer lattice defined by the set of integer vectors $\mathbf{n}$, and let $\Lambda_K$ denote the sampling sublattice generated by the subsampling matrix $\mathbf{K}$, that is the set of integer vectors $\mathbf{m}$ such that $\mathbf{m} = \mathbf{Kn}$. Note that in order to properly define a sublattice of $\Lambda$, a subsampling matrix must be nonsingular with integer-valued entries. In general, a sublattice of $\Lambda$ is called separable if it can be represented by a diagonal matrix $\mathbf{K}$, otherwise it is called nonseparable. Figure 2 shows an integer sampling lattice $\Lambda$ and a sampling sublattice $\Lambda_K$, for the separable subsampling matrix

$$\mathbf{K} = \begin{bmatrix} 2 & 0 \\ 0 & 2 \end{bmatrix}. \tag{8}$$

With $\Lambda$ and $\Lambda_K$ defined this way, we can view the operations of upsampling and downsampling as follows:

- The process of upsampling maps a signal on $\Lambda$ to a new signal that is nonzero only at points on the sampling sublattice $\Lambda_K$. The output of an upsampler is related to the input by

$$y(\mathbf{n}) = \begin{cases} x(\mathbf{K}^{-1}\mathbf{n}), & \text{if } \mathbf{K}^{-1}\mathbf{n} \in \Lambda, \\ 0, & \text{otherwise.} \end{cases}$$

It is easy to show [27] that the Fourier transform relates the output and input of an upsampler by

$$Y(\boldsymbol{\omega}) = X(\mathbf{K}^{\mathrm{T}}\boldsymbol{\omega}),$$

where $X(\boldsymbol{\omega})$ is defined as in (3). Figure 3 shows the block diagram of an upsampler and the process of upsampling for the subsampling matrix defined on (8).

- The process of downsampling maps points on the sublattice $\Lambda_K$ to $\Lambda$ according to

$$y(\mathbf{n}) = x(\mathbf{Kn}), \tag{9}$$

and discards all other points. We can show [27] that the Fourier transform relates the output and input of an downsampler by

$$Y(\boldsymbol{\omega}) = \frac{1}{|\det \mathbf{K}|} \sum_{l=0}^{|\det \mathbf{K}|-1} X(\mathbf{K}^{-\mathrm{T}}(\boldsymbol{\omega} - 2\pi \mathbf{k}_l)),$$

where each of the $|\det \mathbf{K}|$ vectors $\mathbf{k}_l = [k_{l_1}\ k_{l_2}]^{\mathrm{T}}$ is associated with one of the cosets of $\mathbf{K}^{\mathrm{T}}$. Notice that a coset of a sublattice $\Lambda_K$ is defined as the set of points obtained by shifting the entire sublattice by an



Downloaded from SPIE Digital Library on 30 Aug 2010 to 128.59.161.30. Terms of Use: http://spiedl.org/terms

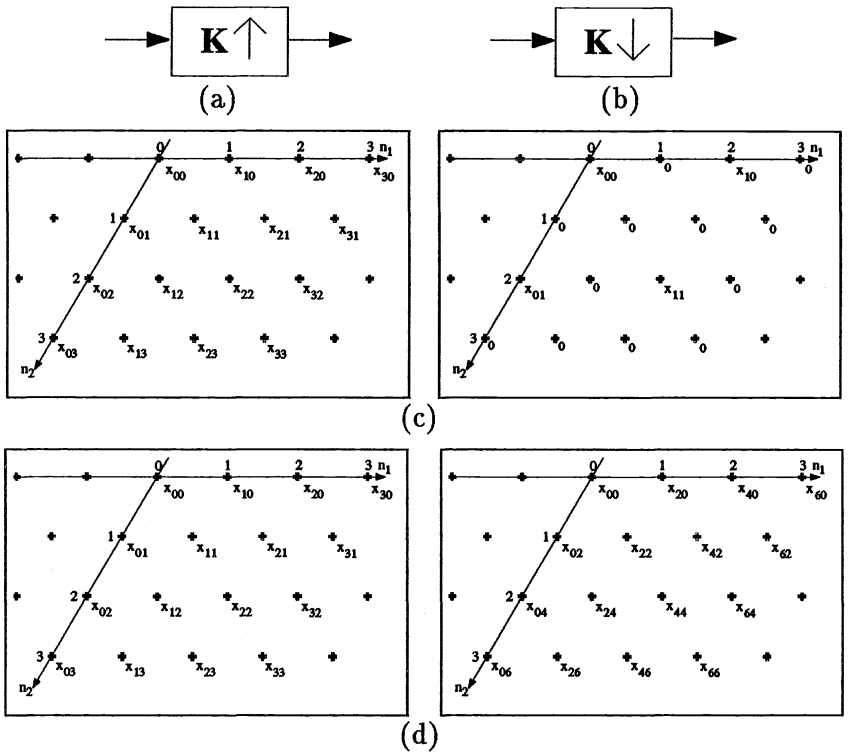


Figure 3: (a) Upsample operator. (b) Downsample operator. Mapping of samples under upsampling and downsampling, (c) and (d) respectively. (Left) input signal, (right) output signal.

integer shift vector $\mathbf{k}$. There are exactly $|\det \mathbf{K}|$ distinct cosets of $\Lambda_{\mathrm{K}}$, and their union is the integer lattice $\Lambda$. Each shift vector $\mathbf{k}_l$ associated with a certain coset is known as a coset vector. For example, one choice for the $\mathbf{k}_l$ given the sampling sublattice defined on (8) is

$$\mathbf{k}_0 = \begin{bmatrix} 0 \\ 0 \end{bmatrix}, \quad \mathbf{k}_1 = \begin{bmatrix} 1 \\ 0 \end{bmatrix}, \quad \mathbf{k}_2 = \begin{bmatrix} 0 \\ 1 \end{bmatrix}, \text{ and } \quad \mathbf{k}_3 = \begin{bmatrix} 1 \\ 1 \end{bmatrix}. \tag{10}$$

Figure 3 shows the block diagram of a downsampler and the process of downsampling for the subsampling matrix defined on (8).

Note that the relations derived above are based on the Fourier transform defined in equation (3). However, a more general definition is described in equation (5). This formulation takes into account the lattice structure used to sample an original 2-D analog waveform an allows the Fourier transform relation between the input and output of an upsampler and a downsampler to be written as

$$Y_{\mathrm{V}}(\mathbf{\Omega}) = X_{\mathrm{V}}(\mathbf{K}^{\mathrm{T}}\mathbf{\Omega}), \tag{11}$$

and

$$Y_{\mathrm{V}}(\mathbf{\Omega}) = \frac{1}{|\det \mathbf{K}|} \sum_{l=0}^{|\det \mathbf{K}|-1} X_{\mathrm{V}}(\mathbf{K}^{-\mathrm{T}}\mathbf{\Omega} - \mathbf{k}_l^h), \tag{12}$$

respectively, where $\mathbf{K}$ is defined as in equation (8) and

$$\mathbf{k}_l^h = \mathbf{U}\mathbf{K}^{-\mathrm{T}}\mathbf{k}_l. \tag{13}$$

In the next section, we consider the analysis/synthesis filter bank problem in hexagonal sampling systems.



Downloaded from SPIE Digital Library on 30 Aug 2010 to 128.59.161.30. Terms of Use: http://spiedl.org/terms

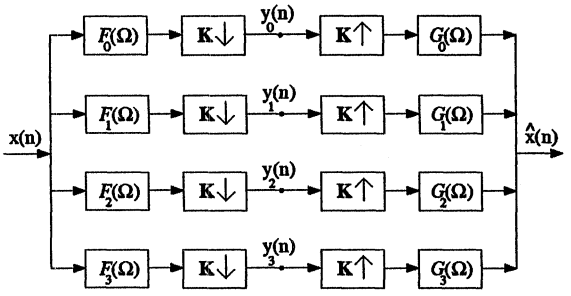


Figure 4: A two-dimensional 4-channel analysis/synthesis filter bank.

## 5. ANALYSIS/SYNTHESIS FILTER BANKS IN HEXAGONAL SYSTEMS

This section focuses on perfect reconstruction filter banks in hexagonal sampling systems and wavelets that can be obtained by iterating such filter banks. Parts of this material are described in Simoncelli [25], but are reviewed here for completeness of presentation.

There are a wide variety of analysis/synthesis (A/S) filter banks for two dimensional systems. In this section we restrict our focus to analysis/synthesis filter banks in which each channel shares the same subsampling matrix $\mathbf{K}$ and the number of channels equals $|\det \mathbf{K}|$. Figure 4 shows a 4-channel analysis/synthesis filter bank. We further restrict our study to the separable sublattice defined in equation (8) since this choice will enable us to apply the A/S filter bank recursively [25] to each of the sub-band signals $y_i(\mathbf{n})$ shown in Figure 4.

Consider a 4-channel analysis/synthesis filter bank with $\mathbf{K}$ defined as in (8), then using (12) we can show that the Fourier transform of $y_i(\mathbf{n})$ may be written as

$$Y_i(\mathbf{\Omega}) = \frac{1}{|\det \mathbf{K}|} \sum_{l=0}^{|\det \mathbf{K}|-1} F_i(\mathbf{K}^{-\mathrm{T}}\mathbf{\Omega} - \mathbf{k}_l^h) X(\mathbf{K}^{-\mathrm{T}}\mathbf{\Omega} - \mathbf{k}_l^h), \tag{14}$$

where the subindex V has been suppressed for simplicity. Similarly, using (11) we have that the Fourier transform of $\hat{x}(\mathbf{n})$ is given by

$$\hat{X}(\mathbf{\Omega}) = \sum_{i=0}^{|\det \mathbf{K}|-1} G_i(\mathbf{\Omega}) Y_i(\mathbf{K}^{\mathrm{T}}\mathbf{\Omega}). \tag{15}$$

Therefore, combining equations (14) and (15) we obtain an overall filter bank response of

$$\hat{X}(\mathbf{\Omega}) = \frac{1}{|\det \mathbf{K}|} \sum_{l=0}^{|\det \mathbf{K}|-1} X(\mathbf{\Omega} - \mathbf{k}_l^h) \left[ \sum_{i=0}^{|\det \mathbf{K}|-1} G_i(\mathbf{\Omega}) F_i(\mathbf{\Omega} - \mathbf{k}_l^h) \right]. \tag{16}$$

Combining equations (7), (10) and (13) for the values of $T_1$ and $T_2$ in equation (2) yields the following set of vectors $\mathbf{k}_l^h$ , that is,

$$\mathbf{k}_0^h = \begin{bmatrix} 0 \\ 0 \end{bmatrix}, \quad \mathbf{k}_1^h = \begin{bmatrix} \pi \\ \frac{\pi}{\sqrt{3}} \end{bmatrix}, \quad \mathbf{k}_2^h = \begin{bmatrix} 0 \\ \frac{2\pi}{\sqrt{3}} \end{bmatrix}, \text{ and } \quad \mathbf{k}_3^h = \begin{bmatrix} \pi \\ \frac{3\pi}{\sqrt{3}} \end{bmatrix}. \tag{17}$$

From equation (17) it is clear that one term of the sum in equation (16) corresponds to the linear shift invariant (LSI) system response, and the remaining terms correspond to the system alias. The analysis/synthesis filter bank for which the system aliasing terms in equation (16) are canceled is generally known as a quadrature mirror filter (QMF) bank.



Downloaded from SPIE Digital Library on 30 Aug 2010 to 128.59.161.30. Terms of Use: http://spiedl.org/terms

We can choose the filters to eliminate the aliasing terms in equation (16)

$$\begin{aligned} F_0(\Omega) &= G_0(-\Omega) = H(\Omega) = H(-\Omega), \\ F_1(\Omega) &= G_1(-\Omega) = \exp(-j\Omega^{\mathrm{T}}\mathbf{s}_1)H(\Omega - \mathbf{k}_1^h), \\ F_2(\Omega) &= G_2(-\Omega) = \exp(-j\Omega^{\mathrm{T}}\mathbf{s}_2)H(\Omega - \mathbf{k}_2^h), \\ F_3(\Omega) &= G_3(-\Omega) = \exp(-j\Omega^{\mathrm{T}}\mathbf{s}_3)H(\Omega - \mathbf{k}_3^h), \end{aligned}$$

where $\mathbf{s}_1$, $\mathbf{s}_2$ and $\mathbf{s}_3$ must satisfy the following equations

$$\begin{aligned} 1 + e^{-j(\mathbf{k}_1^h)^{\mathrm{T}}\mathbf{s}_1} = 0, \quad e^{-j(\mathbf{k}_1^h)^{\mathrm{T}}\mathbf{s}_2} + e^{-j(\mathbf{k}_1^h)^{\mathrm{T}}\mathbf{s}_3} = 0, \\ 1 + e^{-j(\mathbf{k}_2^h)^{\mathrm{T}}\mathbf{s}_2} = 0, \quad e^{-j(\mathbf{k}_2^h)^{\mathrm{T}}\mathbf{s}_1} + e^{-j(\mathbf{k}_2^h)^{\mathrm{T}}\mathbf{s}_3} = 0, \\ 1 + e^{-j(\mathbf{k}_3^h)^{\mathrm{T}}\mathbf{s}_3} = 0, \quad e^{-j(\mathbf{k}_3^h)^{\mathrm{T}}\mathbf{s}_1} + e^{-j(\mathbf{k}_3^h)^{\mathrm{T}}\mathbf{s}_2} = 0. \end{aligned}$$

Therefore, a suitable choice for the vectors $\mathbf{s}_l$ given the vectors $\mathbf{k}_l^h$ in equation (17) is

$$\mathbf{s}_1 = \begin{bmatrix} 1 \\ 0 \end{bmatrix}, \quad \mathbf{s}_2 = \begin{bmatrix} 1/2 \\ \sqrt{3}/2 \end{bmatrix}, \text{ and } \quad \mathbf{s}_3 = \begin{bmatrix} 1/2 \\ -\sqrt{3}/2 \end{bmatrix}.$$

After canceling all of the aliasing terms in equation (16) the remaining LSI system response becomes

$$\hat{X}(\Omega) = \frac{1}{4}X(\Omega)\sum_{i=0}^{3}\left|H(\Omega - \mathbf{k}_i^h)\right|^2.$$

Note that the aliasing cancellation is exact, and independent of the choice of $H(\Omega)$, and the design problem is reduced to finding a filter satisfying the constraint

$$\sum_{i=0}^{3}\left|H(\Omega - \mathbf{k}_i^h)\right|^2 = 4. \tag{18}$$

A low-pass solution for $H(\Omega)$ in the above equation results in a band-splitting system which may be cascaded hierarchically through the low-pass band of the QMF bank to produce a multiresolution decomposition in two dimensions. Simoncelli [25] describes a simple frequency-sampling design method that produces hexagonal QMFs with small regions of support for which perfect reconstruction was well approximated. Figure 5(a) shows an idealized diagram of the partition of the frequency domain resulting from a 2-level multiresolution decomposition of hexagonal filters.

## 6. OVERCOMPLETE MULTIRESOLUTION REPRESENTATIONS IN HEXAGONAL SYSTEMS

In this section we discuss the mathematical formulation of overcomplete multiresolution representations. In particular, we would like to find equivalent filters for the $i^{th}$ stage of the traditional A/S system shown in Figure 5(b).

It can be easily shown that subsampling by $\mathbf{K}$ followed by filtering with $F_0(\Omega)$ is equivalent to filtering by $F_0(\mathbf{K}\Omega)$ followed by subsampling. Hence, the first two steps of low-pass filtering in Figure 5(b) can be replaced by a filter with Fourier transform $F_0(\Omega)F_0(\mathbf{K}\Omega)$, followed by subsampling by $\mathbf{K}^2$.

In general, equivalent filters for the $i^{th}$ stage ($i > 1$) of a cascade of analysis filters are given by

$$F_0^i(\Omega) = \prod_{l=0}^{i-1} F_0(\mathbf{K}^l\Omega), \qquad F_1^i(\Omega) = F_1(\mathbf{K}^{i-1}\Omega)\prod_{l=0}^{i-2} F_0(\mathbf{K}^l\Omega),$$

$$F_2^i(\Omega) = F_2(\mathbf{K}^{i-1}\Omega)\prod_{l=0}^{i-2} F_0(\mathbf{K}^l\Omega), \quad F_3^i(\Omega) = F_3(\mathbf{K}^{i-1}\Omega)\prod_{l=0}^{i-2} F_0(\mathbf{K}^l\Omega),$$



Downloaded from SPIE Digital Library on 30 Aug 2010 to 128.59.161.30. Terms of Use: http://spiedl.org/terms

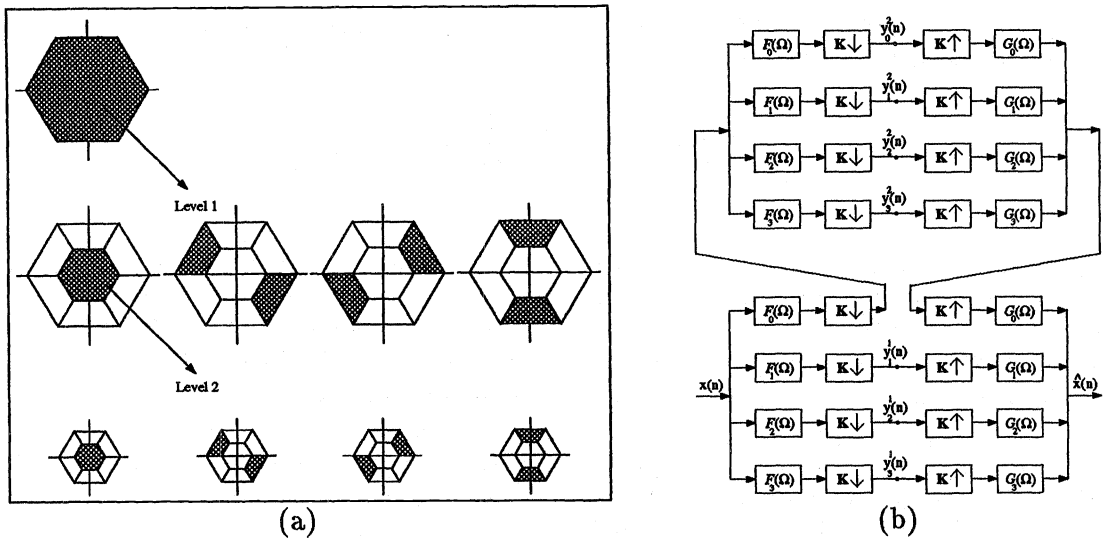


Figure 5: (a) Partitions of the frequency domain resulting from a 2-level multiresolution decomposition using hexagonal filters. The upper left frequency diagram represents the spectrum of the original image. (b) Corresponding two-stage 4-channel analysis/synthesis filter bank.

followed by subsampling by $\mathbf{K}^i$. The synthesis filters are obtained in a similar way. By removing the operations of downsampling and upsampling from the resulting equivalent A/S system we obtain an *over-complete* multiresolution decomposition of hexagonal filters. In this case, perfect reconstruction is also possible from equation (18).

## 7. HEXAGONAL FILTERING FOR RECTANGULARLY SAMPLED IMAGES

In this section we discuss how hexagonal filtering may be applied to rectangularly sampled images. We assume that our original rectangularly sampled images are defined in an $N \times N$ array, where $N$ is some power of 2. To map an original image into a hexagonal sampling lattice we first interpolate the image vertically by a factor of 2 and horizontally by a factor of 3 using bilinear interpolation. The resulting image is then masked by the function $M(\mathbf{n}) = (1 + (-1)^{n_1+n_2})/2$ and mapped into a hexagonal sampling lattice. Filtering was implemented by a hexagonal version of the Fast Fourier Transform (HFFT) [21]. Complete details on our implementation of the HFFT can be found in [24]. After processing, the resulting hexagonal multiresolution decomposition is then mapped back into a rectangular sampling lattice using an interpolation procedure similar to the one outlined above.

## 8. ADAPTIVE MULTIRESOLUTION CONTRAST ENHANCEMENT

In this section we describe a general method to accomplish multiscale contrast enhancement. Let $W_{ij}[x]$ denote the operation of filtering $x(\mathbf{n})$ with the equivalent filter $F_j^i$, where $i$ indicates the level (scale) of the decomposition and $j = 0, 1, 2, 3$ indicates the sub-band filter within each level. Then, the sub-band images of an $L$-level multiresolution decomposition are given by

$$y_j^i = W_{ij}[x]. \tag{19}$$

Similarly, let $W_{ij}^{-1}[y]$ to indicate the operation of filtering image $y(\mathbf{n})$ with the equivalent filter $G_j^i$. Then, an $L$-level multiresolution reconstruction may be written as

$$x = W_{L0}^{-1}[y_0^L] + \sum_{i=1}^{L}\sum_{j=1}^{M} W_{ij}^{-1}[y_j^i]. \tag{20}$$



Downloaded from SPIE Digital Library on 30 Aug 2010 to 128.59.161.30. Terms of Use: http://spiedl.org/terms

By combining equations (19) and (20) we obtain the general expression for an $L$-level multiresolution decomposition and reconstruction

$$x = W_{L0}^{-1}\left[W_{L0}[x]\right] + \sum_{i=1}^{L}\sum_{j=1}^{M} W_{ij}^{-1}\left[W_{ij}[x]\right]. \tag{21}$$

Non-linear techniques for image enhancement may be applied within the context of multiresolution representations. Below we present a general formula for processing sub-band images to accomplish adaptive contrast enhancement of digital mammography. Let $f$ be a user defined function designed to emphasize features of importance within a selected level $i$. Then, enhanced sub-band images $\hat{y}_j^i$ may be given by $\hat{y}_j^i = f(y_j^i)$. Thus, we obtain an enhanced image $\hat{x}$ from its multiresolution representation by replacing in equation (20) selected sub-band images $y_j^i$ with their enhanced counterparts $\hat{y}_j^i$. In particular, the image enhancement techniques described below are applied only to band-pass sub-band images of a multiresolution representation. In general, by defining the function $f$, we can denote specific enhancement schemes for modifying sub-band image coefficients within distinct levels of scale-space.

## 8.1. Local enhancement techniques

A problem for image enhancement in digital mammography is the ability to emphasize mammographic features while *reducing* the enhancement of noise. Multiscale representations localize mammographic features. In [12, 13], we suggested a local enhancement technique for digital mammography based on multiscale edges. Here, enhanced sub-band images $\hat{y}_j^i = f(y_j^i)$ are given by

$$\hat{y}_j^i = \begin{cases} y_j^i, & \text{if } e_j^i \le T_j^i, \\ g_j^i\, y_j^i, & \text{if } e_j^i > T_j^i, \end{cases}$$

where $e_j^i$ is the the edge set corresponding to $y_j^i$, and $g_i$ and $T_j^i$ are the local gain and threshold at level $i$, respectively. Hence, multiscale edges $e_j^i$ are used as an "index" to increase the local gain of sub-band image coefficients and to emphasize significant features "living" within level $i$ of the transform space. Experimentally, we have found that an effective strategy to adaptively select the threshold is to make $T_j^i$ proportional to the standard deviation of pixel values in $y_j^i$, that is

$$T_j^i = \frac{\gamma_1}{N}\sqrt{\sum_{n_1=1}^{N}\sum_{n_2=1}^{N}\left(y_j^i(n_1,n_2) - m_y\right)^2}$$

where $\gamma_1$ is a proportionality constant determined experimentally, $m_y$ is the mean value of $y_j^i$ and $N$ is the size of the image. Notice that for each band-pass image the standard deviation of its pixel values is directly related to the energy of the image within that band. Similarly, $g_j^i$ may be adaptively selected by

$$g_j^i = \frac{\gamma_2}{T_j^i},$$

where $\gamma_2$ is a proportionality constant determined experimentally.

For the hexagonal wavelet transform, sub-band images $y_1^i$, $y_2^i$ and $y_3^i$ partition orientations into 60, 0 and -60 degree bands, respectively. Multiscale edges $e_1^i$, $e_2^i$ and $e_3^i$ at level $i$ are simply obtained by computing the hexagonal-maxima at 60, 0 and -60 degrees, respectively.



Downloaded from SPIE Digital Library on 30 Aug 2010 to 128.59.161.30. Terms of Use: http://spiedl.org/terms

### 8.2. Global enhancement techniques

Histogram equalization of sub-band images provides a global method to accomplish multiresolution enhancement. We simply define the function $f$ as

$$f(y) = \int_{y_{min}}^{y} \rho_y(w)dw + y_{min},$$

where $\rho_y(w) = p_y(w)(y_{max} - y_{min})$, and $p_y(w)$ is the probability density function of $y$. Notice that $f(y)$ is a single-valued, monotonically increasing function in the range $[y_{min}, y_{max}]$ and satisfies $f(y_{min}) = y_{min}$, $f(y_{max}) = y_{max}$.

An advantage of using multiscale analysis for mammographic enhancement is that we can incrementally and selectively focus on features of importance to mammography. If the function $f$ is defined to enhance a single scale, then a focused enhancement of the features "living" within that scale shall be accomplished in reconstruction. We may combine additional representations from any subset of levels and visualize incrementally, mammographic features of specific size and/or shape. Thus, by analogy to current clinical practice, the technique can provide a powerful computational framework for building a computer assisted diagnostic (CAD) tool.

## 9. EXPERIMENTAL RESULTS

Preliminary results have shown that the adaptive multiscale processing techniques described above, can make more obvious unseen or barely seen features of a mammogram without requiring additional radiation. In our study, film radiographs of the breast were digitized at 100 micron spot size, on a Kodak laser film digitizer, with 10-bit quantization (contrast resolution). Each digital image was cropped to a matrix size of $512 \times 512$ before processing.

Figure 6(a) shows a digital mammogram with a large mass. Figure 6(b) shows the result of hexagonal wavelet processing for an eight level decomposition. In this case, the transform coefficients within each level (excluding the DC cap) were independently histogram equalized.

Note that the subtle features including calcifications and penetration of fibroglandular structures into the mass tissue are clearly visible. The geometric shape of calcifications are made more visible and improved definition is seen in the extralobular ductules.

Mathematical models of phantoms were constructed to validate our enhancement techniques against false positives arising from possible artifacts. These models included features of regular and irregular shapes and sizes of interest in mammographic imaging, such as microcalcifications, cylindrical or spiculated objects and conventional masses. Techniques for "blending" a normal mammogram with the images of mathematical models, were developed. The purpose of these experiments was to test our processing techniques on inputs known "a priori" using mammograms where the objects of interest were deliberately obscured by normal breast tissues. The "imaging" justification for "blending" is readily apparent; a cancer is visible in a mammogram because of its (slightly) higher X-ray attenuation which causes a lower radiation exposure on the film in the appropriate region of a projected image. Figure 7(b) shows an example of a mammogram whereby the mathematical phantom shown in Figure 7(a) has been blended into a clinically proven cancer free mammogram. The image shown was constructed by a judicious choice of multiplication weights, adding the amplitude of the mathematical phantom image followed by local smooth filtering of the resultant combined image.

Figure 7(c) shows the result after reconstructing the mammogram from hexagonal wavelet coefficients modified by multiscale edges identified by the adaptive selection technique described in Section 3.1.3. In this example, local contrast enhancement was obtained for a six level hexagonal wavelet decomposition. Processing of the blended mammogram introduced no noticeable artifacts and preserved the shape of the known mammographic features (calcifications, dominant masses, and spiculated lesions). Areas containing these features in the processed mammogram were cropped and enlarged for clarity. Local (multiscale)



Downloaded from SPIE Digital Library on 30 Aug 2010 to 128.59.161.30. Terms of Use: http://spiedl.org/terms

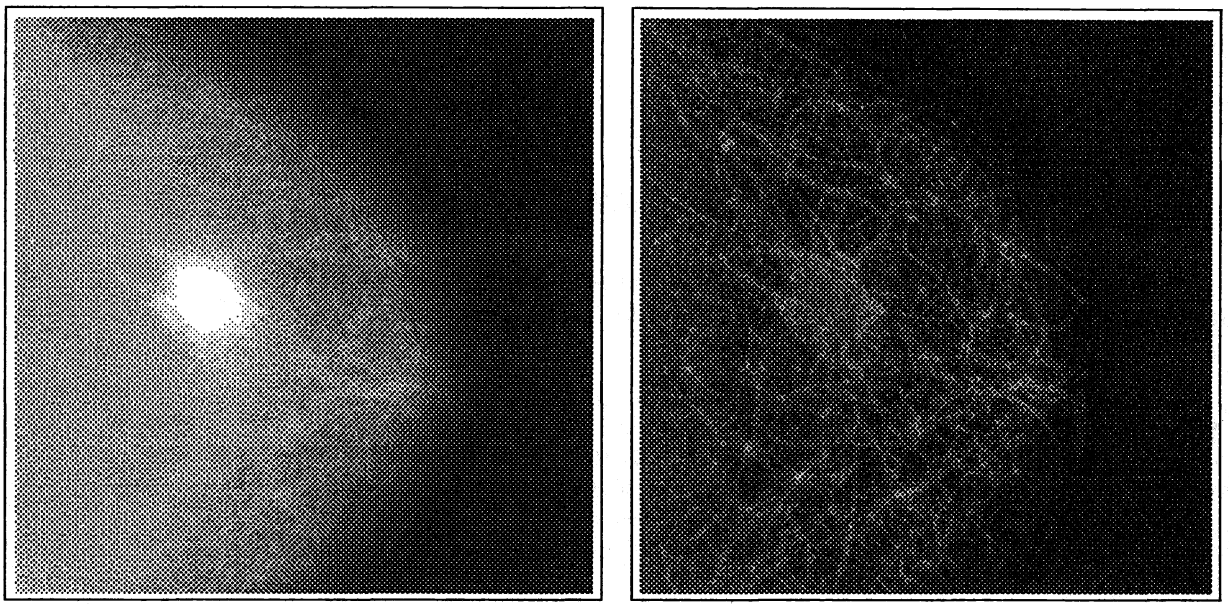

(a) (b)

Figure 6: (a) Mammogram with fibroadenoma. (b) Space-frequency histogram equalization.

emphasis resulted in a significant improvement in contrast for each feature included in the blended mammogram, as shown in Figures 7(d) and 7(e).

While these results are exciting and suggest a strong promise of reliability, we emphasize that they are preliminary. We plan to carry out a more formal analysis including an receiver operator curves (ROC) study in the near future. The study shall include over 350 pathology proven case studies and shall measure the performance of these methods in terms of quality (diagnostic error) and cost (time) for both general radiologist and specialist in mammography.

## 10. SUMMARY AND DISCUSSION

We have presented a methodology for accomplishing adaptive contrast enhancement by multiscale representations. We have demonstrated that features extracted from multiresolution representations can provide an adaptive mechanism for the local emphasis of salient and subtle features in digital mammography. The consistency and reliability suggested by our preliminary studies makes these techniques appealing for computed aided diagnosis and screening mammography. Screening mammography examinations are certain to grow substantially in the next few years, and analytic methods that can assist general radiologists in reading mammograms shall be of great importance.

## 11. ACKNOWLEDGMENTS

This work was sponsored in part by the Whitaker Foundation and the U.S. Army Medical Research and Development Command, Grant number DAMD17-93-J-3003.



Downloaded from SPIE Digital Library on 30 Aug 2010 to 128.59.161.30. Terms of Use: http://spiedl.org/terms

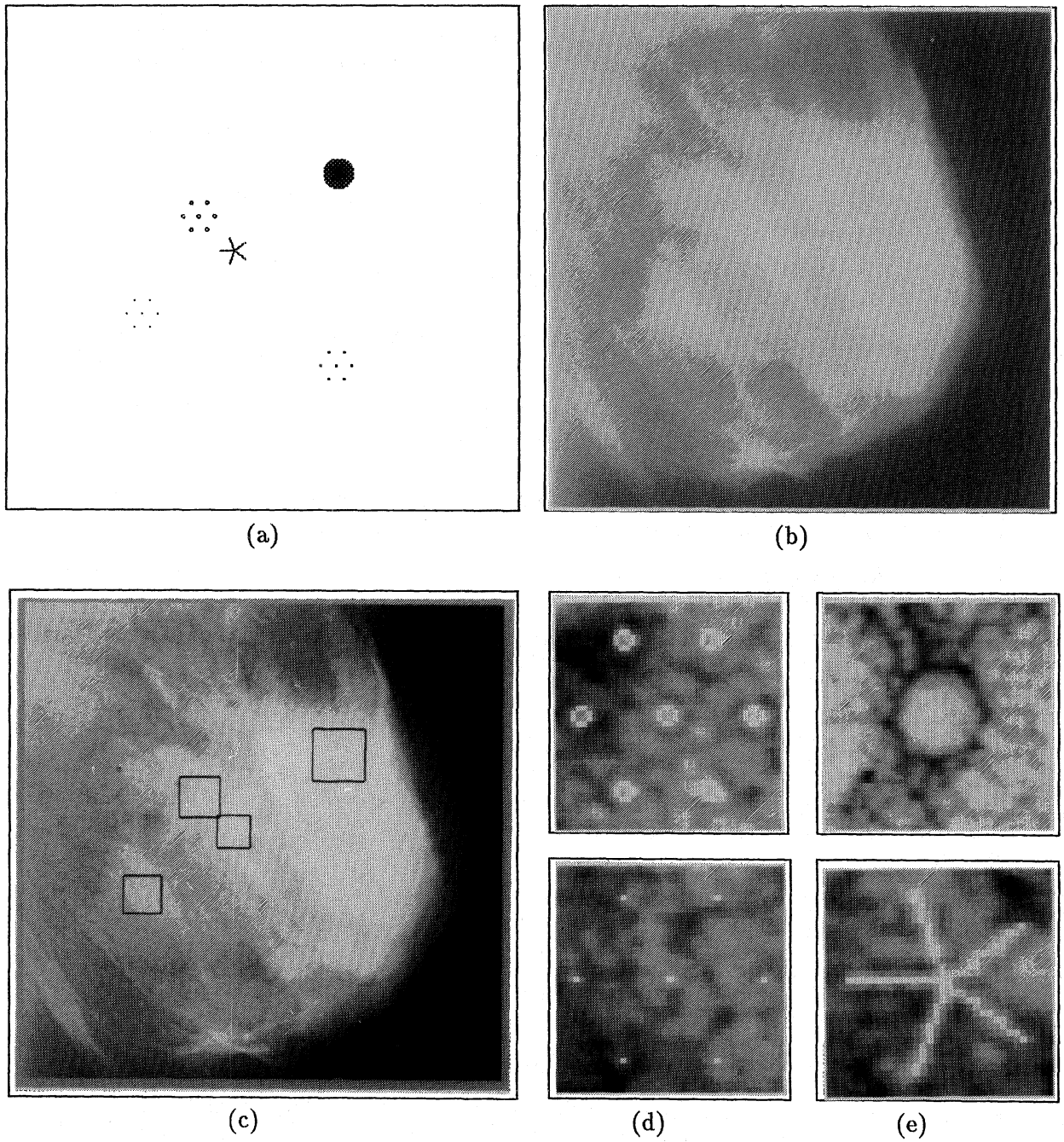


Figure 7: (a) Mathematical phantom. (b) Mammogram M56 blended with phantom. (c) Local enhancement by multiscale edges. (d) Top: circular (arterial) calcification. Bottom: Minute microcalcification cluster. (e) Top: Well circumscribed mass (nodule). Bottom: Spiculated lesion.



Downloaded from SPIE Digital Library on 30 Aug 2010 to 128.59.161.30. Terms of Use: http://spiedl.org/terms

## 12. REFERENCES


[1] I. Brodie, R.A. Gutcheck, "Radiographic information theory and application to mammography," *Medical Physics*, Vol. 9, pp. 79, 1982.

[2] A.C. Bovik, T.S. Huang, D.C. Munson, "The effect of median filtering on edge estimation and detection", *IEEE Transactions on Pattern Analysis and Machine Intelligence,* Vol. PAMI-9, pp. 181–194, 1987.

[3] I. Daubechies, "Orthonormal bases of compactly supported wavelets," *Communications on Pure and Applied Mathematics,* Vol. 41, pp. 909-996, 1988.

[4] I. Daubechies, "The wavelet transform, time-frequency localization and signal analysis," *IEEE Transactions on Information Theory,* Vol. 36(5), pp. 961–1005, 1990.

[5] L.S. Davis, A. Rosenfield, "Noise cleaning by iterated local averaging," *IEEE Transactions on Systems, Man and Cybernetics,* Vol. SMC-8, pp. 705–710, 1978.

[6] A.P. Dhawan, G. Buelloni, R. Gordon, "Enhancement of mammographic features by optimal adaptive neighborhood image processing," *IEEE Transactions on Medical Imaging,* Vol. MI-5, pp. 8, 1986.

[7] A.P. Dhawan, R. Gordon, "Reply to comments on enhancement of mammographic features by optimal adaptive neighborhood image processing," *IEEE Transactions on Medical Imaging,* Vol. MI-6, pp. 82, 1987.

[8] A.P. Dhawan, E. Le Royer, "Mammographic feature enhancement by computerized image processing," *Computer Methods and Programs in Biomedicine,* Vol. 27, pp. 23, 1988.

[9] R. Gorden, R.M. Rangayyan, "Feature enhancement of film mammograms using fixed and adaptive neighborhoods," *Applied Optics,* Vol. 23, pp. 560, 1984.

[10] S.M. Lai, X. Li, W.F. Bischof, "On techniques for detecting circumscribed masses in mammograms," *IEEE Transactions on Medical Imaging,* Vol. MI-8(4), 1989.

[11] A. Laine, "Multiscale wavelet representations for mammographic feature analysis," *Image Enhancement Techniques: Computer Science, National Cancer Institute Breast Imaging Workshop: State-of-the-Art and New Technologies*, Bethesda, MD, September 1991.

[12] A. Laine, S. Song, "Multiscale wavelet representations for mammographic feature analysis," in *Proceedings of SPIE: Conference on Mathematical Methods in Medical Imaging*, San Diego, CA, July 23–25, 1992.

[13] A. Laine, S. Song, "Wavelet processing techniques for digital mammography," in *Proceedings of SPIE: Conference on Visualization in Biomedical Computing,* Chapel Hill, NC, October 13–16, 1992.

[14] A. Laine, S. Song, J. Fan, "Adaptive Multiscale Processing for Contrast Enhancement," to appear in *Proceedings of SPIE: Conference on Biomedical Imaging and Biomedical Visualization,* San Jose, CA, January 31–February 4, 1993.

[15] M. Newman, Integral Matrices, Academic Press, New York, 1972.

[16] S. Mallat, "A Theory for Multiresolution Signal Decomposition: The Wavelet Representation," *IEEE Transactions on Pattern Analysis and Machine Intelligence,* Vol. 11(7), pp. 674–693, 1989.

[17] S. Mallat, "Multiresolution approximations and wavelet orthonormal bases of $L^2$(R)," *Transactions of the American Mathematical Society,* Vol. 315(1), pp. 69–87, 1989.

[18] S. Mallat, "Multifrequency channel decompositions of images and wavelet models," *IEEE Transactions on Acoustics, Speech, and Signal Processing,* Vol. ASSP-37(12), pp 2091–2110, 1989.

[19] S. Mallat, S. Zhong, "Signal characterization from multiscale edges," in *10th International Conference on Pattern Recognition,* Atlantic City, New Jersey, June 1990.




Downloaded from SPIE Digital Library on 30 Aug 2010 to 128.59.161.30. Terms of Use: http://spiedl.org/terms

[20] R.M. Mersereau, D.E. Dudgeon, Multidimensional Digital Signal Processing, Prentice-Hall, Inc., Englewood Cliffs, New Jersey, 1984.

[21] R.M. Mersereau, "The Processing of Hexagonally Sampled Two-Dimensional Signals," *Proceedings of the IEEE*, Vol. 67(6), pp. 930–949 June 1979.

[22] M. Nagao, T. Matsuyama, "Edge preserving smoothing," *Computer Graphics and Image Processing*, Vol. 9, pp. 394–407, 1979.

[23] A. Scheer, F.R.D. Velasco, A. Rosenfiled, "Some new image smoothing techniques," *IEEE Transactions on Systems, Man and Cybernetics*, Vol. SMC-10(3): pp. 153–158, 1980.

[24] S. Schuler, A. Laine, "On discrete processing of hexagonally sampled signals," University of Florida, Computer and Information Sciences Department, Technical Report TR-93-009, 1993.

[25] E.P. Simoncelli, E.H. Adelson, "Non-separable Extensions of Quadrature Mirror Filters to Multiple Dimensions," *Proceedings of the IEEE*, Vol. 78(4), pp. 652–663, April 1990.

[26] P.G. Tahoces, J. Correa, M. Souto, C. Gonzalez, L. Gomez, J. Vidal, "Enhancement of chest and breast radiographs by automatic spatial filtering," *IEEE Transaction on Medical Imaging*, Vol. MI-10(3), pp. 330–335, 1991.

[27] E. Viscito, J.P. Allebach, "The Analysis and Design of Multidimensional FIR Perfect Reconstruction Filter Banks for Arbitrary Sampling Lattices," *IEEE Transactions on Circuits and Systems*, Vol. 38(1), pp. 29–41, January 1981.

[28] T. N. Wiesel, "Postnatal development of visual cortex and the influence of environment (Nobel Lecture)", Nature, Vol. 299, pp. 583–591, 1982.



Downloaded from SPIE Digital Library on 30 Aug 2010 to 128.59.161.30. Terms of Use: http://spiedl.org/terms